CrystEngComm

PAPER

View Article Online
View Journal | View Issue

Cite this: *CrystEngComm*, 2014, **16**, 1472

Crystalline nanoparticle aggregation in non-aqueous solvents†

Nathan D. Burrows,‡[ab] Ellina Kesselman,[b] Kairat Sabyrov,[a] Amanda Stemig,[a] Yeshayahu Talmon[b] and R. Lee Penn*[a]

Received 9th August 2013,
Accepted 7th October 2013

DOI: 10.1039/c3ce41584h

www.rsc.org/crystengcomm

The aggregation of suspended metal oxide and oxyhydroxide nanoparticles dramatically changes as a function of solvent properties. In addition, solvent selection can offer an additional parameter for controlling aggregation and aggregative crystal growth (*e.g.*, oriented aggregation). Here, results are presented demonstrating dramatic changes in the aggregation state of goethite (α-FeOOH), anatase (TiO_2), and ferrihydrite ($Fe_5HO_8{\cdot}4H_2O$) nanoparticles as a function of changing solvents. Results are discussed in the context of Derjaguin and Landau, Verwey and Overbeek (DLVO) theory, additional dynamic light scattering data, and solvent properties like dielectric constant and coordinative ability. Generally speaking, solvents that strongly coordinate the metal oxide/oxyhydroxide surfaces produce the smallest and least compact aggregates, whereas those that weakly coordinate produce the largest and most compact aggregates. Dielectric constant and the nanoparticle morphology are also important factors that impact aggregation state.

Introduction

Direct imaging of nanoparticles in suspension using cryogenic transmission electron microscopy (cryo-TEM) has yielded fundamental insight into the mechanisms of crystal growth and aggregation. For example, cryo-TEM provided evidence supporting a proposed mechanism of amorphous aggregate formation prior to MFI zeolite crystallization, and points to the importance of intra-aggregate rearrangements in nucleation and growth.[1] Through cryo-TEM, new information into prenucleation clusters, their structure, and their fusion within transient aggregates to form amorphous calcium carbonate has been learned.[2] Cryo-TEM has also provided the means to elucidate the structure of an intermediate in oriented aggregation, a secondary structure composed of aligned crystallites separated by *ca.* 1 nm wide spaces, presumably filled with solvent and dissolved species.[3] Cryo-TEM has also been used to characterize the reversibility of aggregation as a function of changing solution conditions.[4] These insights were possible because cryo-TEM enables direct characterization of aggregation state by avoiding introduction of drying artifacts during sample preparation for conventional TEM.

A number of materials, such as goethite[1,3,5–8] and anatase,[9–13] have been shown to grow by oriented aggregation. In this crystal growth mechanism, nanoparticles reversibly aggregate to form secondary structures that are composed of primary particles, which are initially not directly bonded to one another. Rather, there are solvent molecules (and possibly other dissolved species) residing in the spaces between primary particles. They are in constant motion, with their relative orientations fluctuating.[4,14] When the primary particles within one of these structures are crystallographically aligned with respect to one another, the structure has been termed a mesocrystal.[3] The spaces between primary particles are still filled with solvent molecules and possibly other dissolved species, but the crystallites are in crystallographic registry with respect to each other. This mesocrystal can then convert to a single crystal, if the species residing in the spaces between primary particles are either removed or incorporated into the solid crystal structure.

Changing solution conditions such as pH,[4,8,15–18] ionic strength,[7,17,19–21] and molecular additives[4,22] can dramatically affect the kinetics of aggregation as well as crystal growth by oriented aggregation. Previous work has shown that pH strongly affects aggregation before mesocrystal formation, *i.e.*, during earliest stages of growth by oriented aggregation.[4]

The choice of solvent is expected to offer an additional parameter for controlling aggregation and aggregative crystal

[a] *Department of Chemistry, University of Minnesota, 207 Pleasant Street SE, Minneapolis, MN 55455, USA. E-mail: rleepenn@umn.edu; Fax: +1 612 626 7541; Tel: +1 612 626 4680*

[b] *Department of Chemical Engineering and the Russell Berrie Nanotechnology Institute (RBNI), Technion-Israel Institute of Technology, Haifa 32000, Israel*

† Electronic supplementary information (ESI) available. See DOI: 10.1039/c3ce41584h

‡ Current Address: Department of Chemistry, School of Chemical Sciences, University of Illinois, 600 S Mathews, Urbana, IL 61801, USA

growth mechanisms (*i.e.*, oriented aggregation). Here, results demonstrating dramatic changes in aggregation state of metal oxide and oxyhydroxide nanoparticles as function of changing solvents are presented. Four solvents were selected from dozens of candidates: water, isopropyl alcohol (IPA), tetrahydrofuran (THF), and acetic acid (AA). These solvents were selected with four primary concerns in mind. First, the interaction of the solvent molecules with the metal oxide surface. Second, the influence of solvent properties on particle–particle interactions. Third, the probability that high quality cryo-TEM samples could be prepared. And fourth, the compatibility of each solvent with the dialysis membrane. Dielectric constant, dipole moment, and viscosity for each of the four solvents are tabulated in Table 1.[23]

Molecules and coordinating ligands that strongly adsorb to nanoparticles can slow and even inhibit aggregation.[4] However, weakly adsorbing but sufficiently coordinating molecules may be key to facilitating the reorientation of nanoparticles relative to each other during crystal growth by oriented aggregation. It has been suggested that water molecules between closely spaced (*ca.* 1 nm) nanoparticles can mediate particle–particle interactions.[24,25] Therefore, properties such as dipole strength and the degree to which a particular solvent molecule can coordinate with surface sites is also likely to be important. The ability to coordinate is a difficult property to quantify. Neither ligand field splitting nor the logarithmic acid dissociation constant (pK_a) provide an adequate measure of the coordinating ability of a solvent molecule or an anion.[26,27] However, Díaz-Torres and Alvarez have attempted to index the coordinative character of a variety of solvents and anions towards transition metals. Their indexing is based on the probability that a particular solvent molecule will coordinate (or complex with) a transition metal ion, as compared to simply finding that molecule as a part of the transition metal's solvation sphere.[26] Out of the four solvents employed here, water is ranked the most coordinative, followed by IPA and AA, with THF ranked the least coordinative. Furthermore, the coordinative nature of IPA, AA, and THF are expected to be greater with oxides and oxyhydroxides suspended in neat solvent *versus* an aqueous suspension containing each solvent as solute because water displaces IPA, AA, or THF, as it is the stronger coordinating molecule.[26,27]

Besides coordinating with the surface of the nanoparticle, the chemical properties of the solvent are expected to influence particle–particle interactions. Models of oriented aggregation based on Derjaguin and Landau, Verwey and Overbeek (DLVO) theory provide guidance as to which solvent properties may be the most important during initial growth, such as dielectric constant and viscosity.[7,28,29] DLVO theory predicts that the rate of aggregation should increase as, for example, viscosity decreases. This is because the viscosity of the solvent influences the rate of diffusion of the nanoparticles. Using the Stokes–Einstein relation, which calculates the diffusion of spherical particles by Brownian motion,[7,29] decreasing the viscosity proportionally increases the rate of diffusion, all other factors being equal. Furthermore, DLVO based models also lead to a prediction that decreasing dielectric constant will result in a decrease in the repulsive interaction potential energy between nanoparticles, which is expected to lead to increased aggregation. Comparing the non-aqueous solvents employed here to water, both IPA and AA have higher viscosities, but much lower dielectric constants, leading to a prediction of increased aggregation. However, THF has both lower viscosity and dielectric constant relative to water, suggesting that the nanoparticles will aggregate the most in THF as compared with water, IPA, and AA.

Successful characterization of aggregation in nonaqueous solvent requires careful attention to sample preparation. First, the drying or centrifugation of materials from the growth or synthesis media must be avoided, as these techniques, with the goal of separating the product particles from liquid media, can cause irreversible aggregation and other irreversible changes. Here, dialysis of suspensions against neat solvents was performed instead of drying or centrifugation to transfer the material to the new solvents. The liquid medium in which the particles are prepared must be miscible with the target solvent, and both must be compatible with the dialysis membrane. Care must be taken, however, that the particles of interest are not dissolved or partially dissolved during the dialysis step, as was observed during dialysis of suspensions containing partially crystallized particles of zeolite (structure type MFI).[1,30]

An additional consideration is the probability that the selected solvent can be vitrified, which means that a solid glass forms rather than crystalline material, upon plunging into a cryogen. A recent and very successful example of nonaqueous cryo-TEM is its application to study the phase diagram of single-walled carbon nanotubes suspended in chlorosulphonic acid for the production of macroscopic materials.[31] Previous research had shown that branched and functionalized organic molecules can be more readily vitrified than linear hydrocarbons because liquid nitrogen can provide a sufficient cooling rate for branched and functionalized organic molecules,[32] whereas, ethane with its increased cooling rate is required for some molecules (*e.g.*, water). In fact, an amorphous film of a pure, linear hydrocarbon sample has yet to be successfully produced with a cryogen into which the hydrocarbon does not dissolve.

This report describes the direct characterization of the earliest stage of crystal growth by oriented aggregation – the initial aggregation state. Suspensions of ferrihydrite, goethite, or anatase nanoparticles in water, IPA, THF, and AA were prepared, vitrified, and then characterized using cryo-TEM.

Table 1 Solvent properties for acetic acid, isopropyl alcohol, tetrahydrofuran, and water

Solvent	Dielectric constant	Dipole moment	Viscosity
Acetic acid	6.2	1.74 D	1.22 cP
Isopropyl alcohol	18	1.66 D	1.90 cP
Tetrahydrofuran	7.5	1.75 D	0.48 cP
Water	80	1.85 D	1.002 cP

Experimental methods

Material synthesis

Ferrihydrite nanoparticles were prepared following previously published procedures. In a typical synthesis, 50 mL of 0.40 M ferric nitrate (Fisher Scientific, 98+%) and 50 mL of 0.48 M sodium bicarbonate (Sigma Aldrich, 99.7%) were combined by peristaltic pump over a 10.5 min period at a constant temperature of 75 °C. After the addition, the blood-red suspension was rapidly cooled to room temperature by plunging the sealed bottle into an ice water bath with swirling. Then, the suspension was microwave annealed in 40 s intervals to boiling (typically 2 to 3 intervals) in a conventional household microwave oven (950 W, Samsung). The suspension was swirled for a few seconds between irradiation intervals. The suspension was then rapidly cooled to room temperature by swirling in an ice bath. Previous research had shown that this microwave anneal step improves the homogeneity of product crystals.[33]

Goethite nanoparticles were synthesized according to Anschutz and Penn.[34] In summary, ferrihydrite was first prepared, as above, followed by three days of dialysis with ultrapure 18 MΩ cm resistivity water (Milli-Q, Millipore) three times per day. The ferrihydrite suspension was adjusted to pH 12 with 4 M NaOH (Mallinkrodt Chemicals, 99%) and was aged at 90 °C for three days, at which point, the nanoparticles had settled to the bottom of the bottle. The supernatant was discarded and the remaining suspension was dialyzed for three days, again, changing the water three times per day. The particles were left in suspension with Milli-Q water, adjusted to pH 4 with 4 M HNO_3 (Mallinkrodt Chemicals, 68–70%) to inhibit particle aggregation, and left under continuous stirring. The mass per unit volume of the goethite suspension was determined in a simple drying experiment to be 14.5 mg goethite mL^{-1} suspension.

Anatase nanoparticles were synthesized using a modified version of Ye *et al.*[35] and Dai *et al.*[36] The anatase nanoparticles were synthesized using a simple hydrothermal method by hydrolyzing titanium(IV) isopropoxide (Aldrich, 97%) in an acetic acid solution. First, an acetic acid solution was prepared by adding 1 mL of Milli-Q water into 10 mL of acetic acid (Aristar, 99.9%). Then, at room temperature, 0.2 mL of titanium(IV) isopropoxide was added to the acid solution. Just after the addition white flocculates of titanium species were formed indicating the fast hydrolysis of the titanium precursor at these experimental conditions. However, previous work had shown that white titanium species dissolve more easily with increasing solution temperature. The resultant solution was transferred into a 23 mL autoclave bomb (Parr Instrument), and aged in an oven for 20 hours at 200 °C. Then, the suspension was allowed to cool naturally to room temperature.

Small-scale dialysis

Aliquots of nanoparticle suspension were then dialyzed against each target solvent with a 10 : 1 target ratio of solvent to suspension. Dialysis was employed to replace the water with each selected solvent instead of drying or centrifuging followed by suspending in the new solvent because drying or centrifuging can induce substantial changes in aggregation or structure. Dialysis was performed on a small scale to minimize solvent waste. Modified 15 mL centrifuge tubes, modified 1.5 mL microcentrifuge tubes, O-rings, and Spectra/Por 7 dialysis tubing (MWCO 2000 Da) were employed. The hinged lids of the microcentrifuge tubes were removed, and holes matching the outer diameter of the microcentrifuge tubes were drilled into the screw caps of the 15 mL centrifuge tubes. Two 1.5 mL samples of each nanoparticle suspension (ferrihydrite, goethite or anatase) were dialyzed against ~15 mL of AA (Aristar, 99.9%), IPA (Macron Fine Chemicals, 99.9%), THF (Sigma-Aldrich, 99.9%) or water (Milli-Q, 18 MΩ cm resistivity). The latter served as the control experiment. A 1.5 mL aliquot of suspension was placed in a microcentrifuge tube. Then, a small sheet of dialysis membrane (*ca.* 2 cm × 2 cm) was laid across the suspension filled microcentrifuge tube, and secured in place using an O-ring. Then, the 15 mL centrifuging tube was filled to the brim with dialyzing solvent (AA, IPA, THF or water). The microcentrifuge tube was then inverted into the screw cap so that the dialysis membrane separated the suspension from the target solvent. This was carefully done so that (i) the dialysis membrane was in contact with the solvent, (ii) the centrifuge tube remained full of solvent, and (iii) no air bubbles were trapped against the dialysis membrane. Then, the lid to the 15 mL centrifuge tube was screwed over the microcentrifuge tube, securing it in place. Finally, this juncture between the centrifuge tubes was wrapped in parafilm to minimize solvent evaporation. A schematic of this assembly can be seen in Fig. 1. The dialyzing solvent was changed six times over a 48 h period, and the dialysis membrane and O-ring was replaced during each solvent exchange, as both would slowly degrade while in contact with the target solvent; replacement

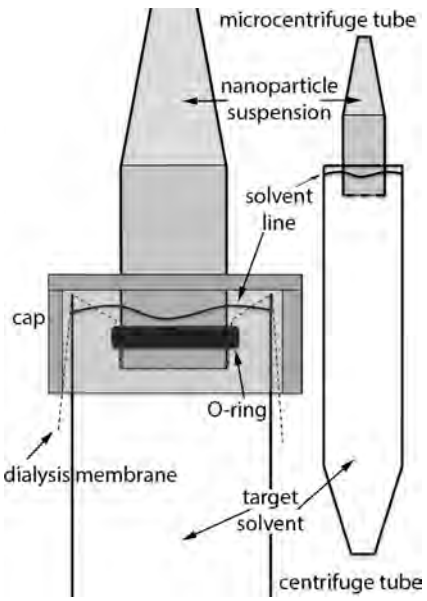

Fig. 1 Schematic of equipment assembly for small-scale dialysis.

ensured no leaks. After dialysis, the two samples of each nanoparticle suspension for each dialyzing solvent were combined and diluted to 25 mL with the dialyzing solvent. Cryo-TEM samples were prepared from these diluted suspensions, which were also analyzed using dynamic light scattering and phase analysis light scattering.

The water content of the post-dialysis suspensions is estimated to be less than 100 parts per billion assuming 1) complete equilibrium across the dialysis membrane between each dialyzing solvent change, 2) no absorption of water from the atmosphere, and 3) no water present in the as-received solvent. According to the product specification/certificate of analysis for these solvents, only THF was tested for water content by Karl Fischer titration ($\leq$0.002%, ~25 parts per million). Assuming all the impurity in AA or IPA was due to water, the maximum water content would be approximately 1 part per thousand. As such, the contribution of water from the initial aqueous suspension would fall below the detection resolution by Karl Fischer titration.[37–40] Thus, the final water content for the suspensions in AA, THF, and IPA were assumed to be similar to that of the as-received solvents.

Cryo-TEM

Cryo-TEM samples were prepared using a controlled environment vitrification system (CEVS), which is designed to control temperature and vapor saturation.[41] The CEVS was employed here due to concern that the nonaqueous solvents could cause damage to the plastic components of a Vitrobot. In addition, vitrification was performed in a fume hood in order to prevent unnecessary exposure to solvent vapor. The CEVS was prepared at 25 °C with two beakers containing 30 mL of the target solvent. 200 mesh copper TEM grids coated with a lacey carbon support film were pretreated for 1 minute by glow discharge prior to loading the grid into the CEVS. Then a drop of the nanoparticle suspension was placed on the front of the grid with a pipette, followed by blotting the backside of the grid with filter paper to thin the drop to a thin film across the lacey carbon. Then the grid was plunged through the trap door of the CEVS into a bath of liquid cryogen. Liquid ethane was used for water and AA specimens, and liquid nitrogen was used for IPA and THF specimens. Then specimens were transferred to a sample storage box in liquid nitrogen until they could be examined.

Specimens were imaged using an FEI Tecnai T12 TEM microscope operated at 120 kV and equipped with a LaB_6 electron source or a FEI Tecnai G2 F30 microscope operated at 300 kV and equipped with a field emission electron source. Images were recorded using a Gatan cooled charge-coupled device (CCD) camera, and low-dose techniques to minimize electron beam induced artifacts.

In addition to artifacts related to atmospheric water vapor,[42–44] non-aqueous cryo-TEM samples are especially susceptible to beam damage, which not only alters the sample but also makes application of electron diffraction techniques challenging. Of the three non-aqueous solvents employed here, IPA is the least sensitive, followed by AA and THF. IPA samples can easily burn from over exposure resulting in bubble/void formation as well as solvent crystallization (ESI,† Fig. S1). AA samples are usually mostly amorphous, but can also contain some acicular crystals of AA that can be easily mistaken for the sample of interest. These crystals can be sublimed under the correct temperature conditions, damaged by beam-induced radiolysis, and found in pure AA samples confirming that these crystals are in fact artifacts of sample preparation (ESI,† Fig. S2). THF samples are by far the most susceptible to radiolysis, and crystallization of the film (ESI,† Fig. S3). Images of artifacts from previously unsuccessful sample preparations are provided in the Electronic Supplementary Information as a resource for those in the scientific community attempting cryo-TEM with these solvents.

Images reported in this paper are modified only in linear adjustments to brightness and contrast across the entire image to exploit the entire range of available gray scale values. Image processing and analysis was conducted using ImageJ (1.46p), an open-source image processing and analysis program written in Java by Wayne Rasband at the U.S. National Institutes of Health.[45–47] Average dimensions of each nanoparticle were determined by measuring multiple particles by hand from calibrated images using the line drawing tool in ImageJ. Aggregate compactness was semi-quantitatively estimated by determining the number of nanoparticles per projected area of the aggregate. This was done by enclosing the aggregate in the smallest convex polygon to determine the projected area of the aggregate. The number of particles in an aggregate was determined by either 1) counting the number of nanoparticles in the aggregate for small aggregates or 2) estimating the number of particles in an aggregate following previously established methods for large aggregates.[7,8]

Dynamic light scattering and phase analysis light scattering

Suspensions of nanoparticles were characterized using dynamic light scattering (DLS) and phase analysis light scattering (PALS) in order to examine *in situ* particle size and zeta potential, respectively. Samples were analyzed using a Brookhaven Zeta PALS Zeta Potential analyzer with 90Plus/BI-MAS Multi Angle Particle Sizing Option equipped with a 657 nm laser using 10 mm polystyrene cuvettes for water, AA, and IPA samples and quartz cuvettes for THF samples. DLS measurements were performed ten times for each suspension. The results were than averaged and analyzed using Brookhaven's Multimodal Size Distribution software to determine an intensity-weighted size distribution, from which a number-weighted size distribution was calculated. PALS measurements were performed ten times with 20 voltage cycles each, averaged, and analyzed using the Smoluchowski method provided in Brookhaven's software to determine zeta potential. THF samples were not analyzed using PALS, as the solvent would have damaged the casing on the PALS probe.

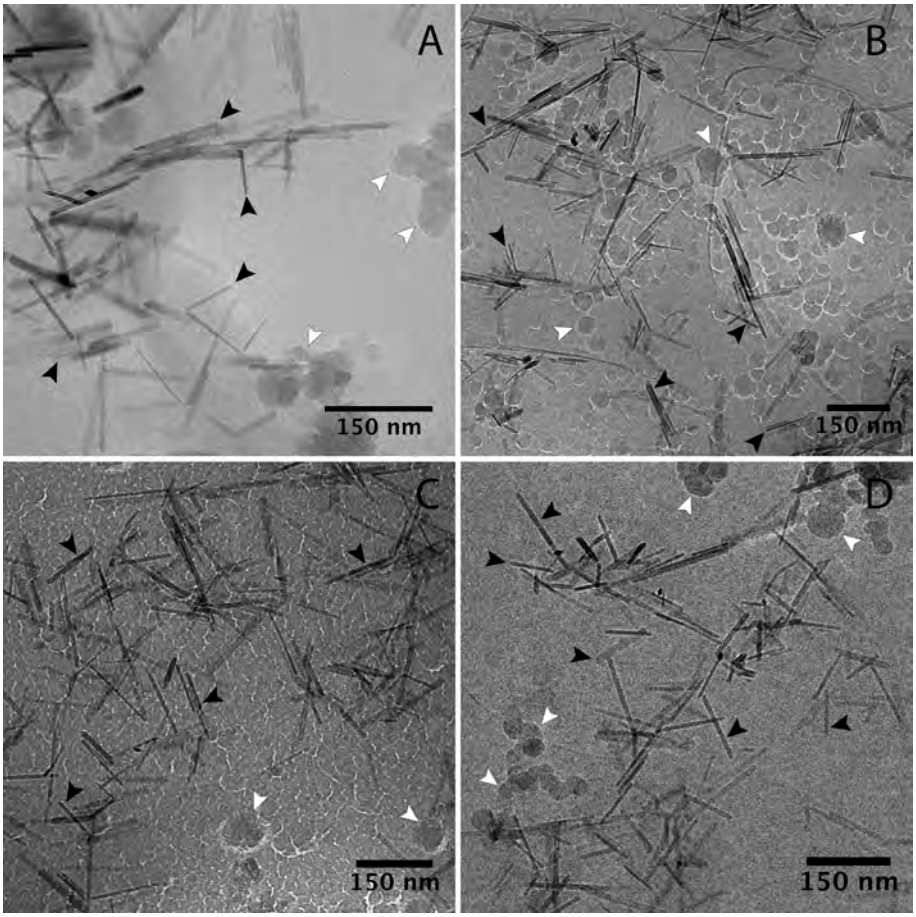

Fig. 2 Cryo-TEM images of goethite nanorods (black arrows) suspended in A) water, B) acetic acid, C) isopropyl alcohol, and D) tetrahydrofuran. Surface contamination (*i.e.*, frost) is identified by white arrows.

Results and discussion

Goethite nanoparticles suspended in water, AA, IPA, and THF form aggregates of dramatically varying size and appearance. Fig. 2 presents representative cryo-TEM images of goethite nanoparticles suspended in water, AA, IPA, and THF. The goethite nanoparticles have an average length of 100 ± 39 nm and average width of 11.5 ± 4.1 nm (n = 517). In water there appear to be very few, if any, isolated nanoparticles, with many particles aggregated side-by-side such that their long axes are parallel to one another. Most goethite nanoparticles form aggregates of a few hundred nanometers in diameter, but some form extended networks over a thousand nanometers in diameter. Aggregates in AA are similar in appearance to aggregates in water, but their aggregate size is typically smaller. Aggregates in IPA, in contrast, are less compact, and exhibit a far smaller fraction of nanoparticles in parallel arrangements with their neighbors, and are almost twice the size found in water. Finally, aggregates in THF appear somewhat more compact than aggregates in IPA, but are substantially larger in size.

Image analysis of the distribution of acute angles formed by the aggregation of nanorods is presented for each solvent in Fig. 3. In water, the most common angle formed by aggregated rods is less than 5°. Substituting AA for water results in an increase in the frequency of angles greater than 5°. Transferring the goethite nanoparticles to IPA or THF changes the most common angle from less than 5° to somewhere in the range of 50–65°.

Fig. 4 presents the number-weighted size distribution of goethite aggregates in each solvent as measured using DLS. These DLS results are consistent with cryo-TEM observations of increasing aggregate size as the coordinative ability of the solvent decreases. Fig. 4 also presents the experimental zeta potentials for suspensions in water, AA, and IPA. No consistent trend between aggregate size and zeta potential is observed, though the goethite particles remain positively charged in water, AA, and IPA.

As with the goethite samples, the size of anatase aggregates increases with the following order: water < IPA < AA < THF. Representative cryo-TEM images of anatase nanoparticles suspended in water and IPA (Fig. 5) and AA and THF (Fig. 6) are presented below. The anatase nanoparticles have an average length of 26.9 ± 4.9 nm and an average width of 16.9 ± 3.5 nm (n = 131). The characteristic remnants of anatase growth by oriented aggregation are observed in all four solvents (*e.g.*, arrow in Fig. 5C); however, oriented aggregates most likely formed during the hydrothermal treatment of the particles at

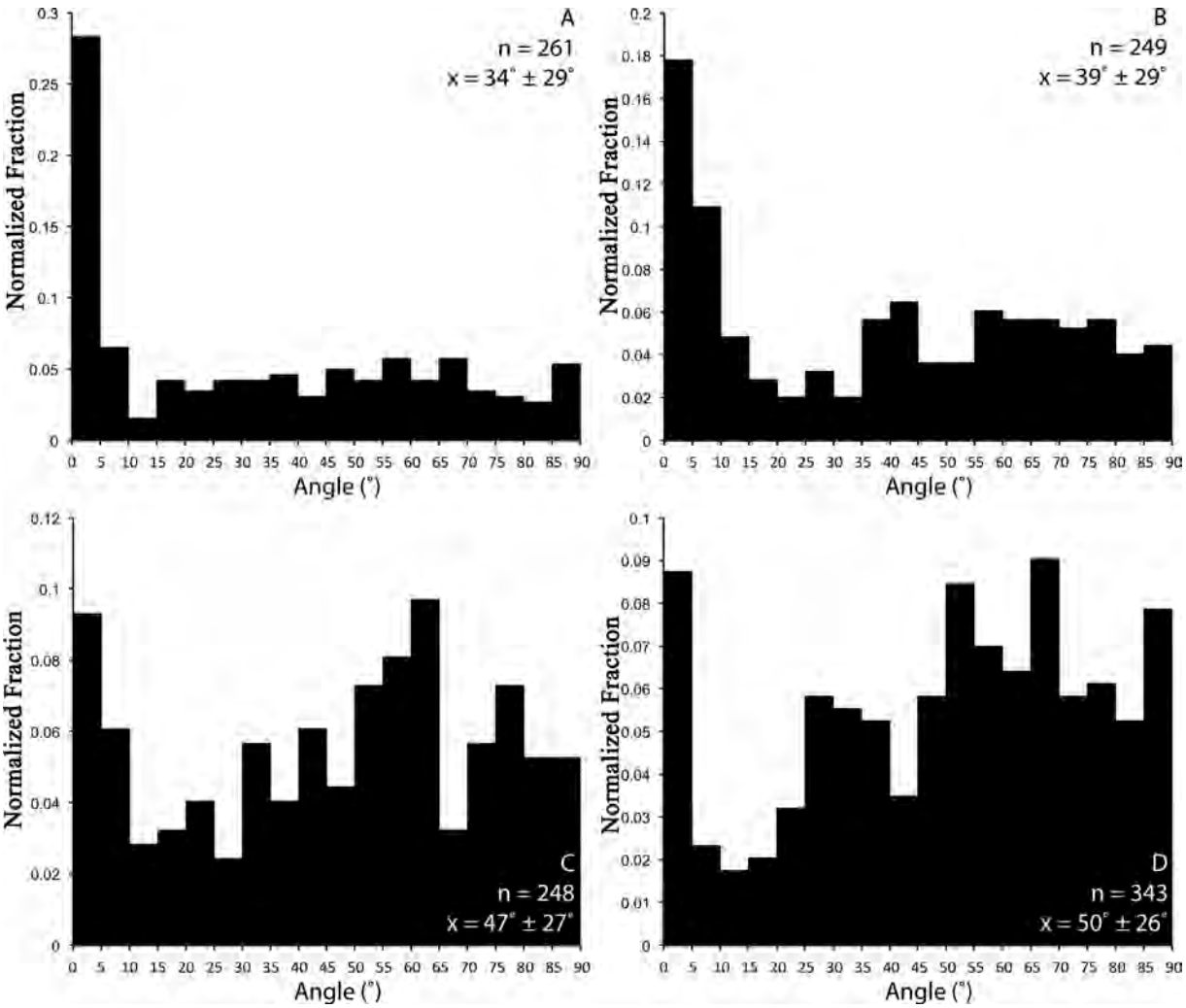

Fig. 3 Histograms of frequency of acute angles between goethite nanorods normalized to the total number of observations in A) water, B) acetic acid, C) isopropyl alcohol, and D) tetrahydrofuran. *n* is the number of angles measured, and *x* is the average angle ± standard deviation.

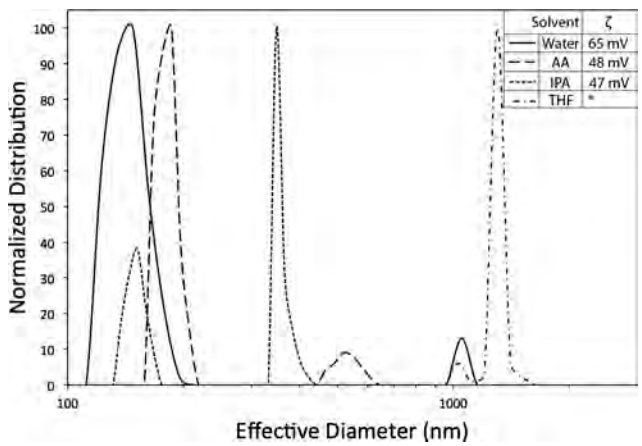

Fig. 4 Number-weighted distributions of goethite aggregate size in water, acetic acid, isopropyl alcohol, and tetrahydrofuran normalized, as measured by DLS, to the most common aggregate size. Zeta potentials are presented in the inset table. *Zeta potential for THF is unavailable due to solvent incompatibility with the instrument probe.

200 °C, which has previously been reported.[11] In water, the anatase crystals most commonly occur in small clusters composed of about 10 to 20 primary particles and occasionally occur as isolated crystallites. In AA, anatase nanoparticles do not appear to be dispersed as well as in water or IPA, forming much larger aggregates that do retain a similar compactness to anatase particles in IPA. Finally, the aggregates observed in THF were the largest and appeared the most compact.

Compactness was semi-quantitatively measured by calculating the two-dimensional (2D) density of particles in images of aggregates. The 2D density for anatase particles in water (15 ± 5 particles per 10^4 nm^2; n = 40), IPA (20 ± 10 particles per 10^4 nm^2; n = 9), and AA (15 ± 5 particles per 10^4 nm^2; n = 4) were similar. In contrast, the 2D density for anatase particles in THF was higher (40 ± 10 particles per 10^4 nm^2; n = 7), supporting the qualitative observation that the aggregates are most compact in THF.

Number-weighted size distributions of anatase aggregates in each solvent from DLS measurements generally agree with observations by cryo-TEM (Fig. 7). Zeta potentials are also

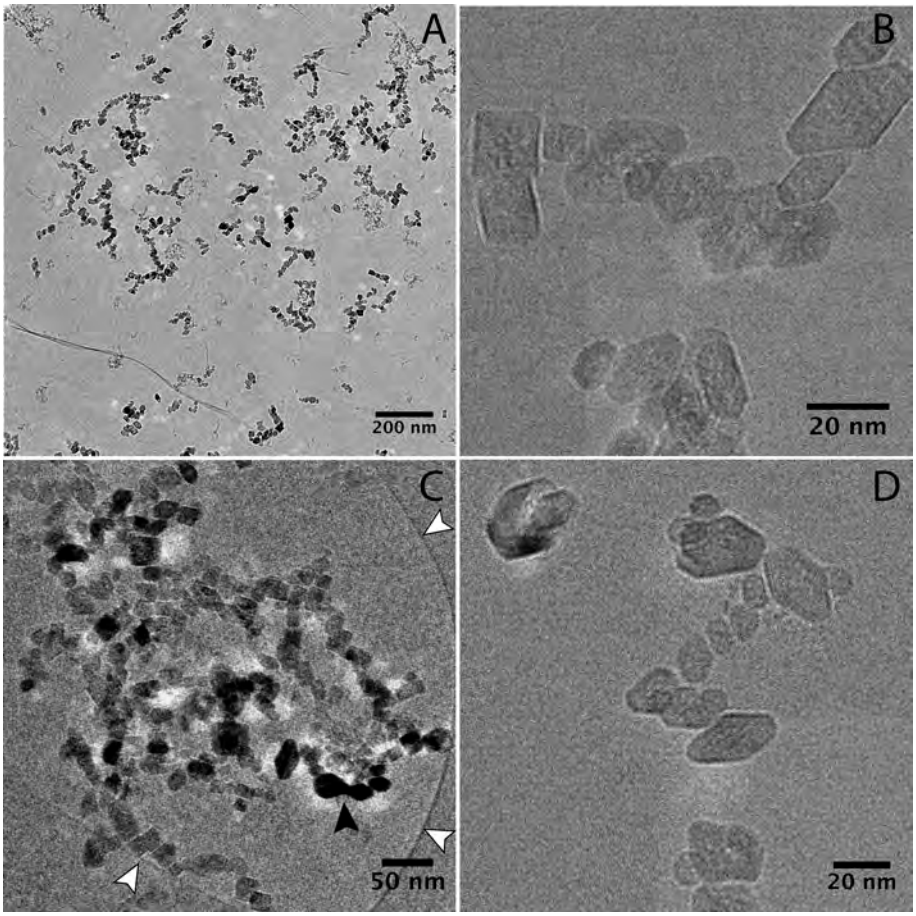

Fig. 5 Images of anatase nanoparticles suspended in A, B) water and C, D) isopropyl alcohol. Black arrow identifies a characteristic morphology of growth by oriented aggregation; white arrows identify the edge of the lacey carbon support film.

presented here. Again, the nanoparticles remain positively charged in each solvent, with those in water the most strongly charged.

As with goethite and anatase suspensions, the size of the aggregates changes dramatically with the change in solvent. However, the effect is more dramatic in the case of the substantially smaller ferrihydrite nanoparticles (6.4 ± 1.3 nm by 4.9 nm ± 1.0 nm; n = 438). Fig. 8 presents representative cryo-TEM images of ferrihydrite nanoparticles suspended in water, IPA, THF, and AA. In water, the ferrihydrite aggregates have structures consistent with previous work that characterized aggregation during early stages of growth by oriented aggregation.[3,4] In IPA, the nanoparticles appear to form very dense spheroid aggregates, which then appear to have aggregated together, but this may be an artifact of blotting during sample preparation. A similar degree of aggregation is observed for ferrihydrite nanoparticles in THF, although the morphology of the aggregates is not spherical, as observed with IPA.

For ferrihydrite, suspensions in AA present a unique characterization challenge due to the small size of the nanoparticle relative to artifacts due to AA crystallization. This makes locating and imaging suspended nanoparticles very difficult. In the very few cryo-TEM observations of ferrihydrite suspended in AA, it appears as though the particles may be well dispersed, with tens of nanometers separating the individual particles.

Number-weighted size distributions obtained from DLS measurements (Fig. 9) generally agree with observations for ferrihydrite suspensions in water, IPA and THF. DLS measurements for ferrihydrite suspended in AA, however, are much larger than observed cryo-TEM. With AA, if the nanoparticles were truly isolated as suggested by the cryo-TEM images, their size would be near the detection limit of the instrument. This weak signal could therefore easily be masked by the presence of even a small amount of larger particles. Therefore, the cryo-TEM results are considered inconclusive at this time. Zeta potential measurements (Fig. 9) are surprising as a charge reversal from positive in water to negative in IPA and AA was observed. The zeta potential is, however, very small for particles suspended in IPA and AA, as compared to water; weak electrostatic repulsion may explain the dense aggregation observed for particles in IPA and is consistent with the DLS results for particles in AA.

When considering all three nanoparticles types in each solvent, two trends become apparent. First, suspensions in water tend to form the smallest aggregates, while suspensions in THF form the largest aggregates. Second, the compactness of the aggregates follows the same order, with

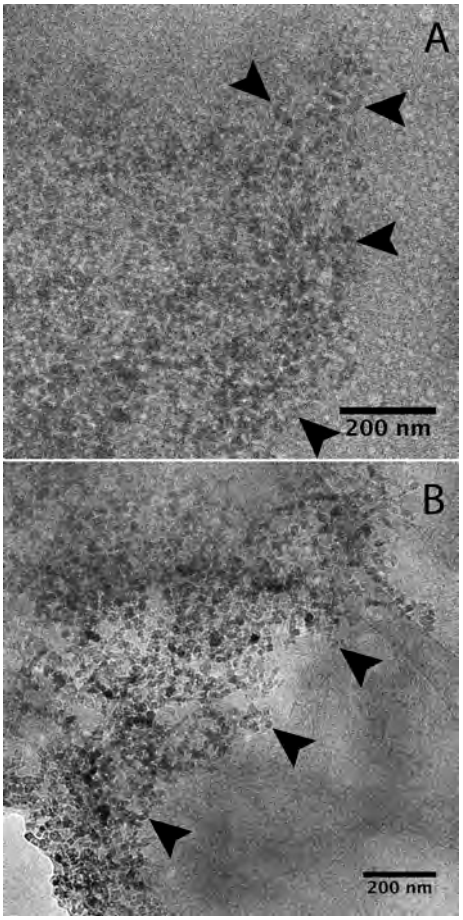

Fig. 6 Cryo-TEM images of anatase particles (black arrows) suspended in A) acetic acid and B) in tetrahydrofuran. The two panels shown represent the best of the images obtained, with most having suitable quality for image analysis but not suitable for publication.

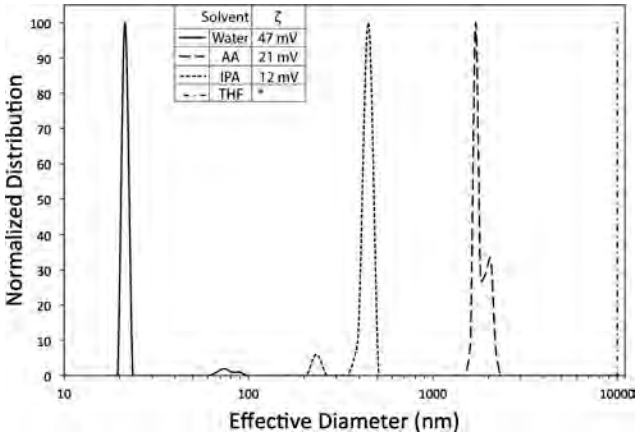

Fig. 7 Number-weighted distributions of anatase aggregate size in water, acetic acid, isopropyl alcohol, and tetrahydrofuran normalized, as measured by DLS, to the most common aggregate size. Zeta potentials are presented in the inset table. *Zeta potential for THF is unavailable due to solvent incompatibility with the instrument probe.

aggregates in water the least compact and aggregates in THF the most. These observations are consistent with nanoparticles in water (compared to the other solvents here) having the highest zeta potential, and therefore highest surface charge density. This trend also appears to follow solvent properties of coordination, dielectric constant, and hydrogen bonding. Of the solvents tested here, water has the highest dielectric constant,[23] the highest coordination ranking with transition metals,[26] and greatest expected hydrogen bonding with the surface; whereas THF has the lowest values for each of these properties. Careful selection of these solvent properties may facilitate formation of loosely aggregated particles that can then reorient under appropriate conditions, to form oriented aggregates, or enable inhibition of aggregative crystal growth.

With goethite, the arrangement of crystals within aggregates seems to coincide with solvent coordination ability. Aggregates formed in AA or water, which are predicted to more strongly coordinate with the metal oxide surfaces, are composed of crystals frequently aligned along the long axes of the rods. However, when in the lower coordinating solvents THF or IPA, the rods appear to be arranged more frequently in starburst-like patterns. Furthermore, dielectric constant appears to be of little significance as both AA and water have very different dielectric constants, and yet form similar structures, whereas AA and THF have very similar dielectric constants and form very different structures.

With anatase, the main difference between solvents is a change in the size of the aggregates, followed by their compactness. Aggregate size increases from water, IPA, AA, to THF. This trend is similar to observations with goethite, except IPA and AA switch order. This change may indicate that dielectric constant plays a larger role at small particle sizes in the aggregation of nanoparticles as the increase in aggregation follows the decrease in dielectric constant.

With ferrihydrite, a dramatic change in aggregate size and the arrangement of nanoparticles in the aggregates was observed when changing the suspending solvent. Aggregates in water are relatively smaller and much more open as compared to their counterparts in IPA or THF. This divide follows both coordinative ability and dielectric constant as water has higher values in both of these properties. These results suggest that smaller nanoparticles are more susceptible to electrostatic, DLVO-based control, where as larger particles are more influenced by the solvent's ability to coordinate with surface of the nanoparticle.

Conclusion

The coordinative character of a solvent appears to have the most substantial effect on the aggregation of oxide and oxyhydroxide particles suspended in neat solvent. The smallest and most open aggregates were observed in water, while the largest and most compact were observed in THF, the molecule expected to have the weakest coordination with the particle surfaces. In addition, the varied size and shape of the particles employed allowed a more detailed elucidation of how solvent properties influence aggregation. With the

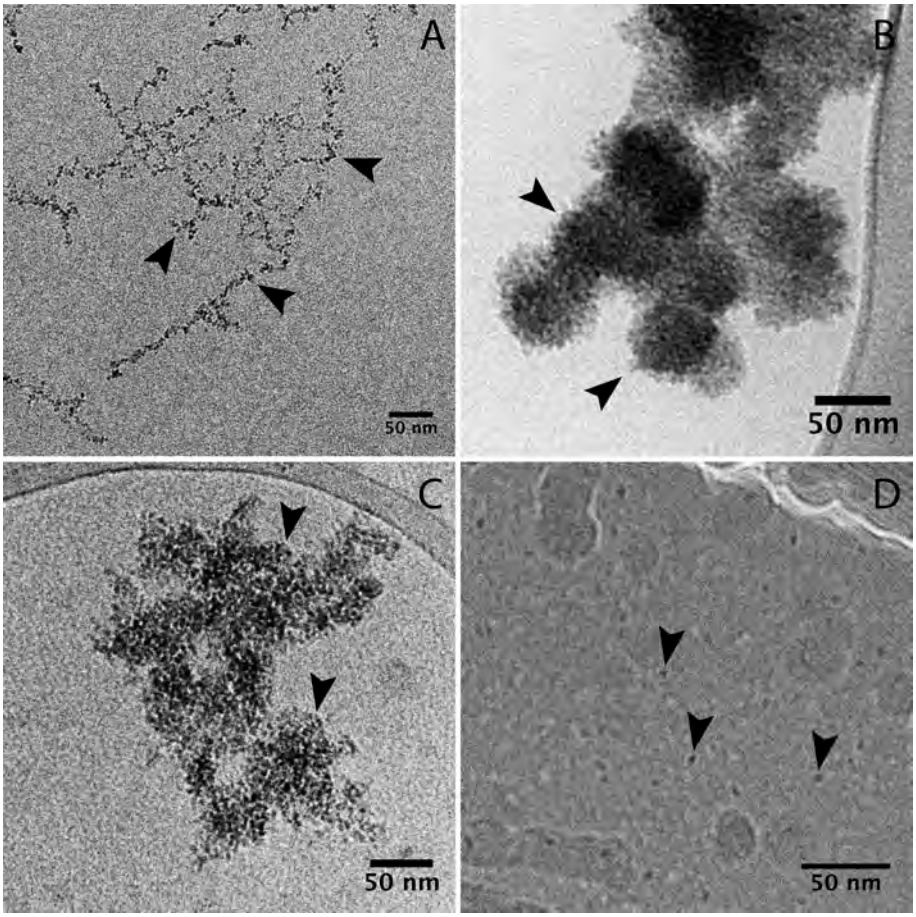

Fig. 8 Cryo-TEM images of ferrihydrite nanoparticles (black arrows) suspended in A) water, B) isopropyl alcohol, C) tetrahydrofuran, and D) acetic acid.

acicular crystals of goethite, an increase in the frequency of side-by-side contacts was observed with the most coordinating solvents. With the very small and nearly spherical ferrihydrite, the trend may more simply be described by DLVO theory. The decrease in dielectric constant and the dramatic observed decrease in surface charge density lead to the predicted increase in aggregation.

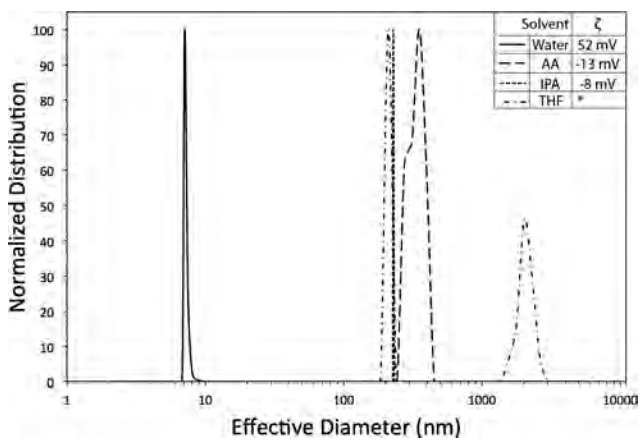

Fig. 9 Number-weighted distributions of ferrihydrite aggregate size in water, acetic acid, isopropyl alcohol, and tetrahydrofuran normalized, as measured by DLS, to the most common aggregate size. Zeta potentials are presented in the inset table. *Zeta potential for THF is unavailable due to solvent incompatibility with the instrument probe.

Non-aqueous cryo-TEM is a challenging technique that requires patience to produce samples of sufficient quality to examine. Through its application here, the role key solvent properties play in the aggregation of metal oxide and oxyhydroxide nanoparticles has been studied. These results are significant from the perspective of crystal growth since aggregation is the first step in nonclassical mechanisms like oriented aggregation and some other particle mediated growth mechanisms. These insights will be helpful in designing aggregation-based nanostructures. Future work will examine the kinetics of crystal growth by oriented aggregation in non-aqueous solvents, as well as mixtures of solvents, to fine-tune control of initial aggregate size and morphology and, thus the properties of the final crystals.

Acknowledgements

We thank the National Science Foundation (NSF-0957696), the University of Minnesota through an International Thesis Research Grant, and the Technion Russell Berri Nanotechnology Institute for financial support. NDB would also like to

thank Judith Schmidt for training in cryo-TEM. Parts of this work were carried out in the Characterization Facility, University of Minnesota a member of the NSF-funded Materials Research Facilities Network and in the Electron Microscopy of Soft Mater Laboratory at the Technion – Israeli Institute of Technology.

References

1 S. Kumar, Z. Wang, R. L. Penn and M. Tsapatsis, *J. Am. Chem. Soc.*, 2008, **130**, 17284–17286.
2 M. Kellermeier, D. Gebauer, E. Melero-García, M. Drechsler, Y. Talmon, L. Kienle, H. Cölfen, J. M. García-Ruiz and W. Kunz, *Adv. Funct. Mater.*, 2012, **22**, 4301–4311.
3 V. M. Yuwono, N. D. Burrows, J. A. Soltis and R. L. Penn, *J. Am. Chem. Soc.*, 2010, **132**, 2163–2165.
4 V. M. Yuwono, N. D. Burrows, J. A. Soltis, T. A. Do and R. L. Penn, *Faraday Discuss.*, 2012, **159**, 235–245.
5 R. L. Penn, J. J. Erbs and D. M. Gulliver, *J. Cryst. Growth*, 2006, **293**, 1–4.
6 R. L. Penn, K. Tanaka and J. J. Erbs, *J. Cryst. Growth*, 2007, **309**, 97–102.
7 N. D. Burrows, C. R. H. Hale and R. L. Penn, *Cryst. Growth Des.*, 2012, **12**, 4787–4797.
8 N. D. Burrows, C. R. H. Hale and R. L. Penn, *Cryst. Growth Des.*, 2013, **13**, 3396–3403.
9 R. L. Penn and J. F. Banfield, *Science*, 1998, **281**, 969–971.
10 R. L. Penn and J. F. Banfield, *Am. Mineral.*, 1998, **83**, 1077–1082.
11 R. L. Penn and J. F. Banfield, *Geochim. Cosmochim. Acta*, 1999, **63**, 1549–1557.
12 S. L. Isley and R. L. Penn, *J. Phys. Chem. C*, 2008, **112**, 4469–4474.
13 G. Oskam, A. Nellore, R. L. Penn and P. Searson, *J. Phys. Chem. B*, 2003, **107**, 1734–1738.
14 D. Li, M. H. Nielsen, J. R. I. Lee, C. Frandsen, J. F. Banfield and J. J. De Yoreo, *Science*, 2012, **336**, 1014–1018.
15 K. Sabyrov, N. D. Burrows and R. L. Penn, *Chem. Mater.*, 2012, **25**, 1408–1415.
16 S. Das, M. J. Hendry and J. Essilfie-Dughan, *Environ. Sci. Technol.*, 2011, **45**, 268–275.
17 R. A. French, A. R. Jacobson, B. Kim, S. L. Isley, R. L. Penn and P. C. Baveye, *Environ. Sci. Technol.*, 2009, **43**, 1354–1359.
18 D. Lee, D. Omolade, R. E. Cohen and M. F. Rubner, *Chem. Mater.*, 2007, **19**, 2382–2382.
19 P. Linton, H. Wennerstrom and V. Alfredsson, *Phys. Chem. Chem. Phys.*, 2010, **12**, 3852–3858.
20 K. M. Mullaugh and G. W. Luther, *J. Nanopart. Res.*, 2011, **13**, 393–404.
21 S. L. Isley, D. S. Jordan and R. L. Penn, *Mater. Res. Bull.*, 2009, **44**, 119–125.
22 C. C. Li, X. M. Yin, Q. H. Li and T. H. Wang, *CrystEngComm*, 2011, **13**, 1557–1563.
23 *CRC Handbook of Chemistry and Physics: a ready-reference book of chemical and physical data*, ed., W. M. Haynes, CRC Press, Boca Raton, FL, 92nd edn, 2011.
24 H. Zhang, B. Gilbert, F. Huang and J. F. Banfield, *Nature*, 2003, **424**, 1025–1029.
25 D. Spagnoli, B. Gilbert, G. A. Waychunas and J. F. Banfield, *Geochim. Cosmochim. Acta*, 2009, **73**, 4023–4033.
26 R. Díaz-Torres and S. Alvarez, *Dalton Trans.*, 2011, **40**, 10742–10750.
27 M. R. Rosenthal, *J. Chem. Educ.*, 1973, **50**, 331.
28 N. D. Burrows, V. M. Yuwono and R. L. Penn, *MRS Bull.*, 2010, **35**, 133–137.
29 S. K. Friedlander, *Smoke, Dust, and Haze: Fundamentals of Aerosol Dynamics*, Oxford University Press, New York, 2nd edn, 2000.
30 Ch. Baerlocher and L. B. McCusker, *Database of Zeolite Structures:* http://www.iza-structure.org/databases/.
31 V. A. Davis, A. N. G. Parra-Vasquez, M. J. Green, P. K. Rai, N. Behabtu, V. Prieto, R. D. Booker, J. Schmidt, E. Kesselman, W. Zhou, H. Fan, W. W. Adams, R. H. Hauge, J. E. Fischer, Y. Cohen, Y. Talmon, R. E. Smalley and M. Pasquali, *Nat. Nanotechnol.*, 2009, **4**, 830–834.
32 D. Danino, R. Gupta, J. Satyavolu and Y. Talmon, *J. Colloid Interface Sci.*, 2002, **249**, 180–186.
33 D. Burleson and R. L. Penn, *Langmuir*, 2006, **22**, 402–409.
34 A. J. Anschutz and R. L. Penn, *Geochem. Trans.*, 2005, **6**, 60–66.
35 J. Ye, W. Liu, J. Cai, S. Chen, X. Zhao, H. Zhou and L. Qi, *J. Am. Chem. Soc.*, 2011, **133**, 933–940.
36 Y. Dai, C. M. Cobley, J. Zeng, Y. Sun and Y. Xia, *Nano Lett.*, 2009, **9**, 2455–2459.
37 K. Fischer, *Angew. Chem.*, 1935, **48**, 394–396.
38 P. Bruttel and R. Schlink, *Metrohm Monograph*, 2003, **8**, 2003–2009.
39 J. Mitchell and D. M. Smith, *Aquametry: a treatise on methods for the determination of water*, Wiley, New York, 2nd edn, 1977.
40 E. Scholz, *Karl Fischer Titration: Determination of Water*, Springer-Verlag, Berlin, English Translation, 1984, vol. 20.
41 J. R. Bellare, H. T. Davis, L. E. Scriven and Y. Talmon, *J. Electron Microsc. Tech.*, 1988, **10**, 87–111.
42 N. D. Burrows and R. L. Penn, *Microsc. Microanal.*, 2013, DOI: 10.1017/S1431927613013354, FirstView Article, 1–12.
43 H. Cui, T. K. Hodgdon, E. W. Kaler, L. Abezgauz, D. Danino, M. Lubovsky, Y. Talmon and D. J. Pochan, *Soft Matter*, 2007, **3**, 945–955.
44 H. Friedrich, P. M. Frederik, G. de With and N. A. J. M. Sommerdijk, *Angew. Chem., Int. Ed.*, 2010, **49**, 7850–7858.
45 M. Abramoff, P. Magelhaes and S. Ram, *Biophotonics International*, 2004, **11**, 36–42.
46 W. S. Rasband, *ImageJ*, U.S. National Institutes of Health, Bethesda, MD, 1st edn, 1997.
47 T. J. Collins, *BioTechniques*, 2007, **43**, 25–30.